Theoretical and Computational Acoustics
D. Lee, Y-H Pao, M.H. Schultz, and Y-C Teng (Editors)

Modeling the Effects of Azimuthal Coupling on Acoustic Propagation in the Presence of 3-Dimensional, Rough Ocean Interfaces Using the Parabolic Approximation

Kevin B. Smith
Department of Physics, Code PH/Sk, Naval Postgraduate School, Monterey, CA 93943

Abstract: In most ocean acoustic propagation models, the uncoupled azimuth approximation is assumed and solutions are generated for the 2-dimensional Helmholtz equation. For 3-dimensional problems, a 2DxN approach is often employed where N is the number of different azimuthal radials along which the standard 2-dimensional solution is computed. Still other models use a hybrid approach, using adiabatic modes to compute the depth dependence and a parabolic approximation to solve for azimuthal variations. Presented here is an algorithm employing a fully 3-dimensional application of the parabolic approximation using the split-step Fourier method to march the solution out in range. The various forms of the depth-dependent potential function are still available, allowing high angle accuracy in vertical wavenumber. The azimuthally-dependent potential function is assumed to be small, thereby limiting its accuracy to small angles of azimuthal scatter. In this sense, the azimuthal dependence is of the "standard PE" type. The UMPE acoustic propagation model has been upgraded to incorporate this algorithm, and is now referred to as UMPE3D. The solutions are marched out in range as before by replacing the 1-dimensional FFT in depth with a 2-dimensional FFT in depth and azimuth. Examples of this will be shown in a realistic ocean environment with a rough bottom interface, and the effects of azimuthal coupling will be discussed.

Introduction

In the early 70's, the parabolic approximation to the Helmholtz wave equation for underwater acoustic propagation was introduced by Tappert (1974). The split-step Fourier method (Hardin and Tappert, 1973) for numerically solving this differential equation was quickly recognized as an extremely efficient means of predicting one-way acoustic propagation. In a thorough description of the parabolic equation approximation, hereafter referred to as PE, Tappert (1977) justified neglecting the azimuthally-variant term, an approach now referred to as the uncoupled azimuth (UNCA) approximation. Since those years, various other schemes have been employed to solve the PE (e.g., Lee and Botseas, 1982; Collins, 1988), and various means of approximating the pseudo-differential square-root operator in the PE formulation have been introduced (e.g., Thomson and Chapman, 1983; Berman et al., 1989). The success of the PE method is evidenced by its incorporation into the Navy standard acoustic propagation model (Holmes and Gainey, 1991). In fact, PE solutions are becoming so accurate and the algorithms so sophisticated, workshops have been conducted to compare these solutions with exact, or "benchmark," solutions (Chin-Bing, et al., 1993). In some simple environments, these workshops showed some PE models capable of accuracy within tenths of dB's. Most, if not all, of these models have assumed the UNCA approximation to be valid.

This paper has two primary purposes. The first is to describe a simple extension of the UMPE model (Smith and Tappert, 1993) which employs the split-step Fourier, hereafter referred to as SSF, algorithm to compute the effects of azimuthal variability. The second is to use this extended version of the UMPE model, or UMPE3D, to examine the validity of the UNCA approximation in a particular environment which contains highly variable bathymetry. Other issues that arise when azimuthal coupling occurs will also be addressed. It should be noted that this research is still preliminary in its results and several issues of consequence to the physics of

underwater acoustic propagation will be left for the reader to ponder.

In Sec. I, a brief description of the basic 2DxN, SSF/PE model used will be described as well as the 3D extension incorporating azimuthal variability. A simple 3D wedge test case and a more complicated, real ocean environment are examined in Sec. II. Some fundamental propagation effects due to azimuthal coupling are addressed in more detail in Sec III. The results are summarized in Sec. IV. Future research directions are also discussed.

I. The acoustic model

We begin with the free-space Helmholtz equation in cylindrical coordinates for the acoustic pressure $p(r, z, \varphi)$,

$$\frac{1}{r}\frac{\partial}{\partial r}\left(r\frac{\partial p}{\partial r}\right)+\frac{1}{r^2}\frac{\partial^2 p}{\partial \varphi^2}+\frac{\partial^2 p}{\partial z^2}+k_0^2 n^2(r, z, \varphi)\, p = 0 \tag{1}$$

where $k_0 = \frac{\omega}{c_0}$ is the reference wavenumber, $n(r, z, \varphi) = \frac{c_0}{c(r, z, \varphi)}$ is the acoustic index of refraction, c_0 is the reference sound speed, and $c(r, z, \varphi)$ is the acoustic sound speed. It is within $c(r, z, \varphi)$ that all features of the environment are represented. We now define the pressure field as

$$p(r, z) = \frac{1}{\sqrt{r}} u(r, z) \quad . \tag{2}$$

The function $u(r, z)$ is identical to the pressure field in two dimensions and the term $\frac{1}{\sqrt{r}}$ accounts for azimuthal spreading. Substituting (2) into the Helmholtz equation yields the far-field expression

$$\frac{\partial^2 u}{\partial r^2}+\frac{\partial^2 u}{\partial z^2}+\frac{1}{r^2}\frac{\partial^2 u}{\partial \varphi^2}+k_0^2 n^2(r, z)\, u = 0 \quad . \tag{3}$$

We introduce the operators

$$P_{op} = \frac{\partial}{\partial r} \tag{4}$$

and

$$Q'_{op} = \left[n^2+\frac{1}{k_0^2}\left(\frac{\partial^2}{\partial z^2}+\frac{1}{r^2}\frac{\partial^2}{\partial \varphi^2}\right)\right]^{1/2} \quad . \tag{5}$$

Eq. (3) then becomes

$$(P_{op}^2 + k_0^2 Q'^2_{op})\, u = 0 \tag{6}$$

which can be factored as

$$(P_{op} + ik_0 Q'_{op})\,(P_{op} - ik_0 Q'_{op})\, u + ik_0 [P_{op}, Q'_{op}]\, u = 0 \quad . \tag{7}$$

The commutator $[P_{op}, Q'_{op}]$ is assumed negligible and is, in fact, exactly zero in layered media. Eq. (7) represents the combination of incoming and outgoing waves. The outgoing wave satisfies

$$-ik_0^{-1}\frac{\partial u}{\partial r} = Q'_{op}u \quad . \tag{8}$$

We now define

$$\varepsilon = n^2 - 1, \quad \mu = \frac{1}{k_0^2}\frac{\partial^2}{\partial z^2}, \quad \text{and} \quad \nu = \frac{1}{k_0^2 r^2}\frac{\partial^2}{\partial \varphi^2} \tag{9}$$

such that

$$Q'_{op} = (\mu + \varepsilon + \nu + 1)^{1/2} \quad . \tag{10}$$

If we assume that the effect of azimuthal coupling is relatively small (since $\frac{\partial}{\partial \varphi}c(r, z, \varphi) \ll \frac{\partial}{\partial z}c(r, z, \varphi)$, in general) then we may expect $\nu \ll \mu + \varepsilon$. Therefore, Eq. (10) may be approximated by

$$Q'_{op} = (\mu + \varepsilon + 1)^{1/2} + \frac{1}{2}\nu = Q_{op} + \frac{1}{2}\nu \tag{11}$$

where

$$Q_{op} = (\mu + \varepsilon + 1)^{1/2} \tag{12}$$

is the usual PE square-root operator. It is the approximation of this pseudo-differential operator that distinguishes many PE models from one another. Note that the approximation used in Eq. (11) can be considered of the "standard-PE" type. However, the approximation ultimately used for Q_{op} is still undetermined and, in fact, can be of any of the commonly used forms.

For the moment, let us neglect azimuthal variability and assume $Q'_{op} = Q_{op}$. We now define the PE field function $\psi(r, z, \varphi)$ according to

$$u(r, z) = \psi(r, z)\, e^{ik_0 r} \tag{13}$$

and obtain

$$\frac{\partial \psi}{\partial r} = -ik_0\psi + ik_0 Q_{op}\psi \quad . \tag{14}$$

In SSF algorithms, the trick is now to develop an approximation for Q_{op} that separates into a z-space operator and a k-space (vertical wavenumber) operator. It is then often convenient to describe this operator in terms of a Hamiltonian operator, i.e.,

$$Q_{op} = 1 - H_{op} = 1 - [T_{op}(\mu) + U_{op}(\varepsilon)] \tag{15}$$

where T_{op} and U_{op} are the "kinetic energy" and "potential energy" operators, respectively.

We now define the z-space and k-space transform pairs according to

$$\psi(z) = \mathrm{FFT}(\hat{\psi}(k)) \tag{16}$$

and

$$\hat{\psi}(k) = [\mathrm{FFT}(\psi^*(z))]^* \quad . \tag{17}$$

The general PE/SSF marching algorithm can then be defined by

$$\psi(r + \Delta r, z) = e^{-ik_0 \Delta r U_{op}(r, z)} \times \mathrm{FFT}\{e^{-ik_0 \Delta r \hat{T}_{op}(r, k)} \times [\mathrm{FFT}(\psi^*(r, z))]^*\} \quad . \tag{18}$$

For all of the work presented here, the "wide-angle" (WAPE) approximation of Thomson and Chapman (1983) is employed. Then

$$U_{WAPE}(r,z) = -[n(r,z)-1] \quad \text{and} \quad \hat{T}_{WAPE}(k) = 1-\left[1-\left(\frac{k}{k_0}\right)^2\right]^{1/2} . \tag{19}$$

To expand this algorithm to include azimuthal variability, we need only add a new operator to the propagation equation which we shall define as

$$V_{op} = -\frac{1}{2k_0^2 r^2}\frac{\partial^2}{\partial\varphi^2} . \tag{20}$$

Analogous to the operator T_{op} in z-space, this operator is not diagonal in φ-space and is therefore not a simple multiplication operator. Just as T_{op} coupled vertical angles of propagation, V_{op} produces a coupling of azimuthal angles. Following the same reasoning as before, we define a variable s as the "wavenumber" analog to the azimuthal bearing φ according to

$$\psi(r,z,\varphi) = \int \hat{\psi}(r,z,k_0 s)\, e^{ik_0 s\varphi} d(k_0 s) = \text{FFT}\left[\hat{\psi}(r,z,k_0 s)\right] . \tag{21}$$

The propagator that couples azimuths is then $e^{-ik_0\Delta r\hat{V}_{op}(r,s)}$ where

$$\hat{V}_{op}(r,s) = \frac{s^2}{2r^2} . \tag{22}$$

We now must examine more closely the explicit calculation of the variable s. To do so, we continue with the analogy to the vertical wavenumber variable k. The incremental values of vertical wavenumber were defined by

$$k = n\Delta k , \quad n = -\left(\frac{N}{2}-1\right), \frac{N}{2} \tag{23}$$

where N is the transform size of the FFT between z-space and k-space, and with

$$\Delta k = \frac{2\pi}{z_T} \tag{24}$$

where z_T is the total computational depth. Since $\Delta z = \frac{z_T}{N}$, it follows that

$$\Delta k \Delta z = \frac{2\pi}{N} . \tag{25}$$

Therefore, if we define M as the transform size between φ-space and s-space then

$$s = m\Delta s , \quad m = -\left(\frac{M}{2}-1\right), \frac{M}{2} \tag{26}$$

with

$$k_0\Delta s = \frac{2\pi}{\varphi_T} \tag{27}$$

and φ_T is the total azimuthal interval in radians (e.g., 2π, $\frac{\pi}{2}$, etc.). The incremental values of azimuth are obviously given by

$$\Delta\varphi = \frac{\varphi_T}{M} \tag{28}$$

so the azimuthal analog to Eq. (25) is

$$k_0 \Delta s \Delta\varphi = \frac{2\pi}{M} \ . \tag{29}$$

To compute the 3-D propagation of a point source, we simply create identical starting fields for each bearing at $\varphi = m\Delta\varphi$. For $\varphi_T < 2\pi$, the entire z-space starting fields should be tapered near the ends, or outermost bearings, near $\varphi = \pm\frac{M}{2}\Delta\varphi$. An explicit horizontal beampattern could also be used to define the φ variability of the starting field. A 2-D FFT between $\psi(r, z, \varphi)$ and $\hat{\psi}(r, k, s)$ is then used in conjunction with a split-step algorithm analogous to Eq. (18) with the operator substitutions

$$U_{op}(r, z) \rightarrow U_{op}(r, z, \varphi) \quad \text{and} \quad \hat{T}_{op}(r, k) \rightarrow \hat{T}_{op}(r, k) + \hat{V}_{op}(r, s) \ . \tag{30}$$

This completes the basic formulation of a fully 3-D PE/SSF model. It should be noted that a similar algorithm was previously used by Baer (1981) in which all operators were of the "standard PE" type.

II. Some examples

In this section, two different environments are considered: a simple, 3-D wedge, and a complicated, deep ocean environment with a rough bottom. The former problem has been studied previously in great detail. Analytical formulations in integral form have been derived by Deane and Buckingham (1993) for such cases. We will not attempt to compare our results with those solutions, however, since even the 2-D SSF/PE solution does not provide accuracy to better than a dB or so. The effects due to azimuthal coupling in this environment are also on this order and would therefore be difficult to compare. However, the basic trend of downslope refraction can be confirmed. The deep ocean problem, on the other hand, has no analytical solution and we shall again rely on expected trends to confirm the results. Both cases have been computed for 512 radials evenly spaced over 360°.

1. The 3-D wedge environment

For an initial test case, a 3-D wedge environment was chosen. This is simply a 2-D wedge extended cross-slope. A simple, point-like source is used at a depth of 100 m at 250 Hz. The depth of the water column at the source position is 1000 m and a constant 1500 m/s sound speed was used. The bottom was a fluid with sound speed 1700 m/s, density contrast of 1.5, and attenuation of 0.85 dB/m/kHz. A slope of 15° was chosen to provide noticeable coupling effects and calculations were made out to a maximum range of 3.5 km. Using the 2DxN (UNCA) version of the model produces the results shown in Fig. 1a. These values represent transmission loss to the bottom interface. The 0° azimuth was chosen as the upslope direction and 180° is downslope. The most noticeable influence of azimuthal coupling is then expected along 90° and 270°.

When azimuthal coupling is included, the results displayed in Fig. 1b are obtained. The two figures are strikingly similar, indicating the influence of azimuthal coupling is not severe. To highlight the influence of azimuthal coupling, the difference between these transmission loss values (a measure of the relative rms intensities) is computed and shown in Fig. 2. As anticipated, the strongest influence is observed away from the direct upslope or downslope directions. A careful analysis of the intermixed increases and decreases in transmission loss reveals that the interference pattern observed is consistent with an overall downslope refractive character.

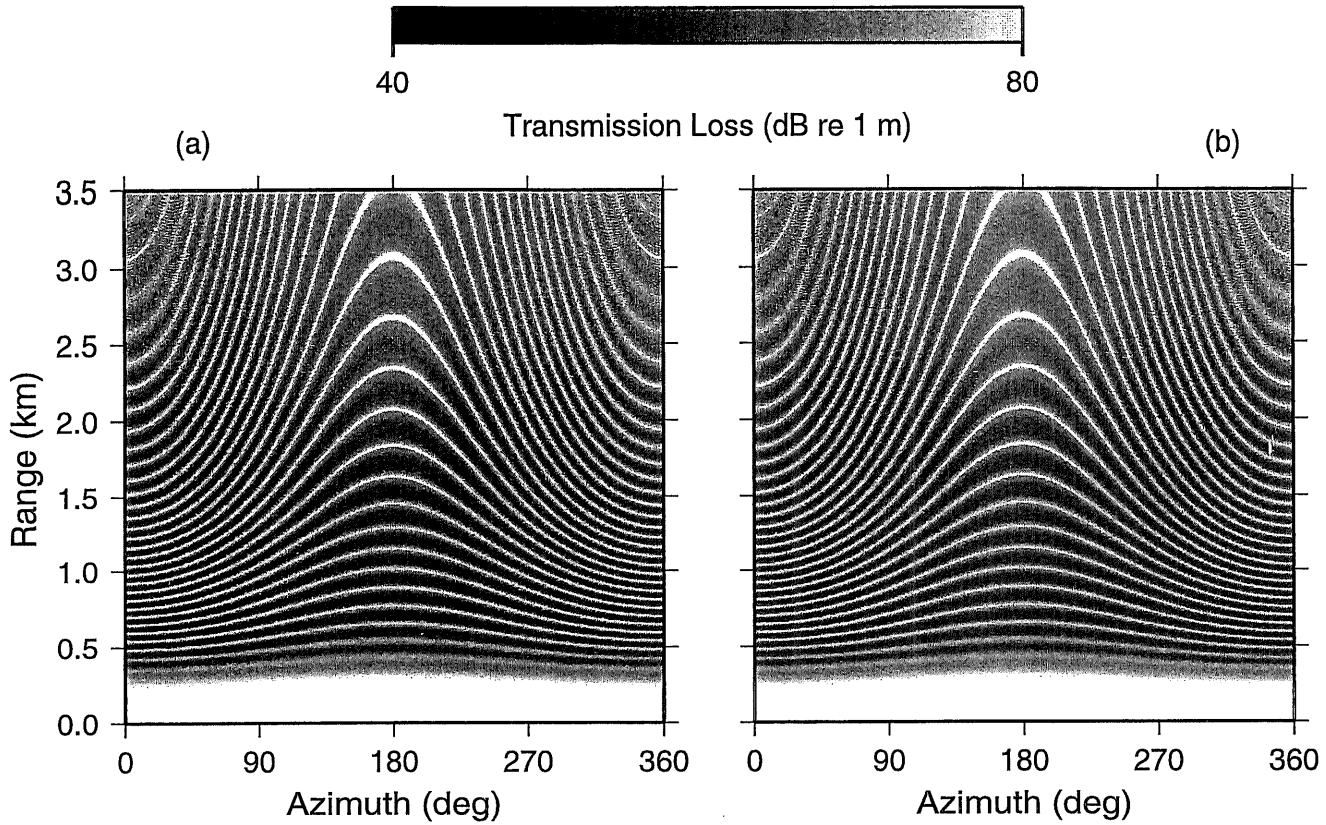

Figure 1: Transmission loss at the bottom interface of a 3-dimensional wedge (a) without azimuthal coupling and (b) with azimuthal coupling.

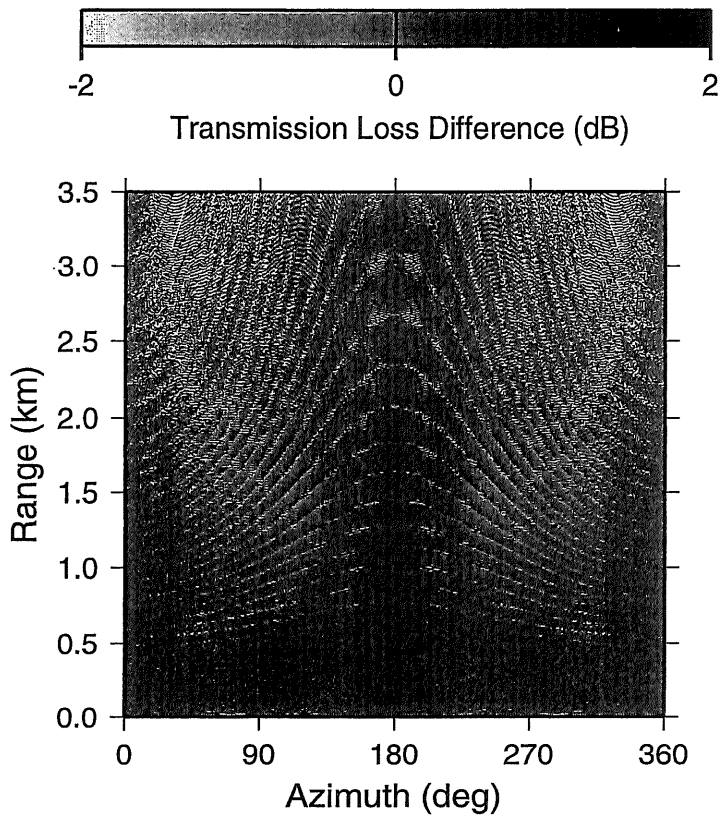

Figure 2: Difference in transmission loss values of Fig. 1(a) and 1(b). Positive values indicate higher TL with azimuthal coupling.

2. Deep ocean, rough bottom environment

In 1990, the Office of Naval Research (ONR) began a Special Research Program (SRP) in the area of underwater acoustic reverberation. A large-scale reconnaissance survey was carried out in July-August 1992 on the R/V Ewing where HMR1 sidescan sonar data and Hydrosweep 15 kHz multibeam bathymetry data were collected (Tucholke et al., 1993). The area covered was approximately 200 km in the north-south direction and 400 km in the east-west direction. The data set used for this work was gridded at 200m x 200m. The acoustic bottom properties are chosen to be representative of this area and have no lateral variability due to lack of geophysical data. A constant bottom sound speed of 1800 m/s, density contrast of 2.0, and attenuation of 0.2 dB/m/kHz were chosen. CTD casts performed during the experiment provide water column sound speed data.

Recorded reverberation from one of the transmitted pings during the experiment is presented in Fig. 3 with bathymetry contours overlaid. The source was a vertical array of approximately 21 m in length and centered at a depth of 181 m. The center frequency for the displayed signal was 227.5 Hz with a 55 Hz bandwidth. The reverberation was recorded by a horizontal array using standard shading to produce a typical horizontal beampattern. The highest resolution was obtained broadside to the array with a 3 dB beamwidth of roughly 1.5 deg while the end-fire beams had a beamwidth of 22 deg. Issues relating to the effects of azimuthal coupling on horizontal beampatterns will be discussed in the following section. Note the left-right ambiguity inherent in the beampattern in Fig. 3.

We now consider the two-way propagation from the source to the bottom interface and back to the receiver with and without the influence of azimuthal coupling. For this analysis, we shall consider only the propagation of the central frequency from a vertical array and observed by a point receiver (i.e., no horizontal beam pattern). The two-way transmission loss to the bottom for this CW calculation without azimuthal coupling is displayed in Fig. 4a. (The data displayed are rescaled to suggest predicted reverberation levels.) The same data from the fully coupled calculation is very similar. The difference between the two transmission loss calculations is shown in Fig. 4b. There are several important characteristics to note. The magnitude of the differences is typically on the order of several dB. However, there doesn't seem to be any particular pattern correlating with bathymetry. Instead, the differences appear as a random, "speckled" pattern. The size of these fluctuations appears to be on the order of 100's of meters and increasing with range. Note that for short ranges (near-field), the differences are barely detectable even though the coupling term, Eq. (22), is expected to be strongest in this region. Presumably, the near-field, direct paths are not distinguishable between the two cases (since all the coupling will be due to bottom interactions). The forward-scattered field, however, which begins to interact at more distant ranges, begins to produce the observable fluctuations. Finally, one may be convinced from the gray-shading of the scale that there is a tendency for lower transmission loss values when azimuthal coupling is included. This issue will be explored further in the next section. These results must be considered with the caveat that the azimuthal resolution is only ~ 0.7 degrees and, therefore, the cross-range resolution at the maximum computational range of 50 km is ~ 200 m. Such resolution may not be adequate to justify any observable trends.

III. Influence on propagation

In this section, results are presented from calculations which have a total azimuthal range of $\varphi_T = 30°$ over 512 radials. To perform this calculation properly using the SSF algorithm, a

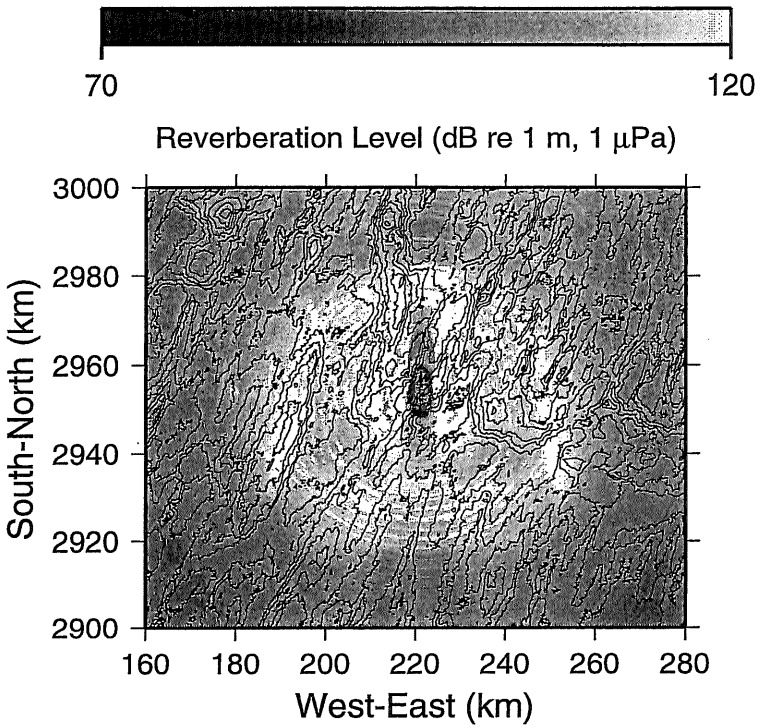

Figure 3: Reverberation returns due to vertical array transmission as measured by horizontal array from ONR-ARSRP study. Bathymetry contours at 250 m intervals are overlaid.

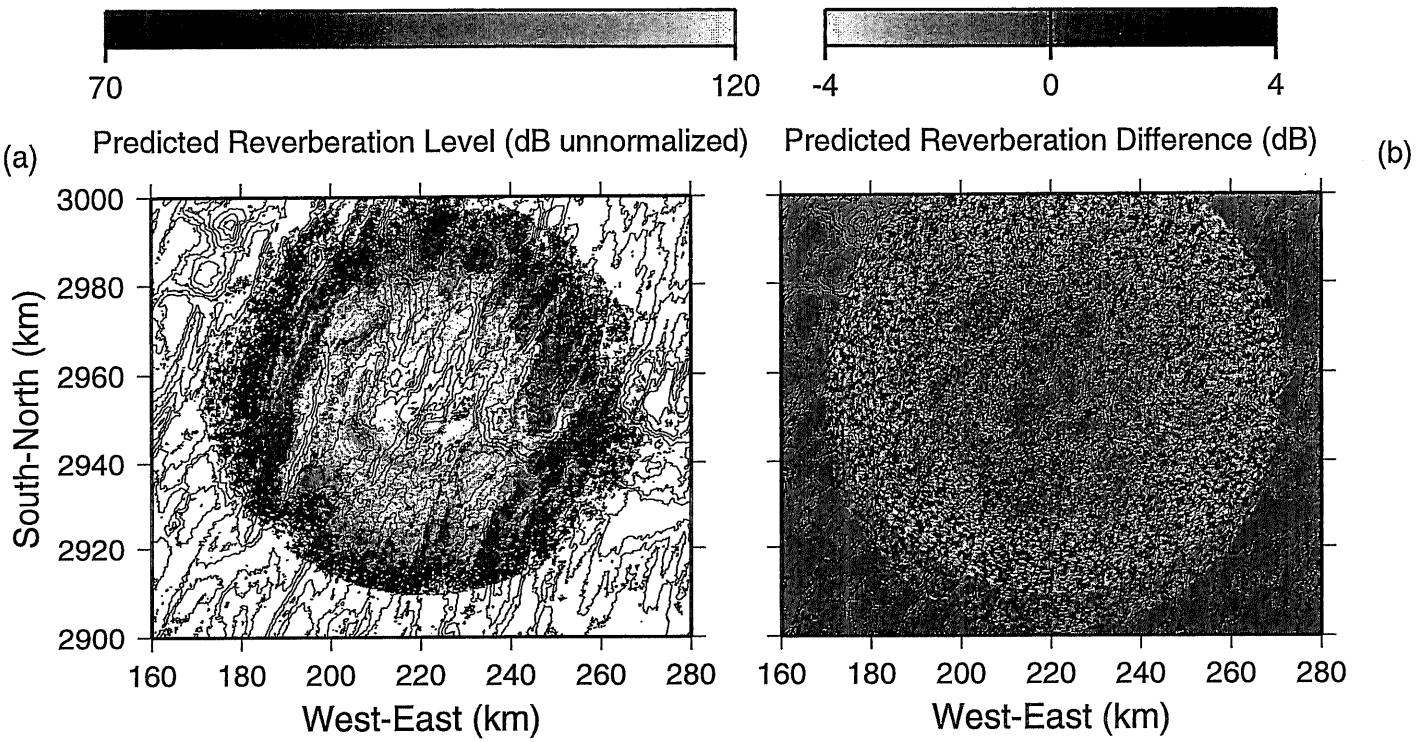

Figure 4: (a) Predicted reverberation levels (rescaled 2-way TL) for modeled environment of Fig. 3 without azimuthal coupling. (b) Difference in 2-way TL predictions. Positive values indicate higher TL with azimuthal coupling. (Note maximum calculation range is 50 km.)

$\cos^2$ filter has been applied over the outer 2/3, leaving the innermost 10° unaffected. This angular resolution now provides a cross-range resolution of ~ 50 m at 50 km which should be adequate if the coupling isn't extreme. We first attempt to examine the issue of average *TL* levels in the presence of azimuthal coupling. The effect on highly focused beams is then considered.

1. Effects on long-range transmission loss

Propagating this 30° "beam" in the same deep ocean, rough bottom environment used in the last section produces the results displayed in Fig. 5a without azimuthal coupling. The introduction of coupling produces the data in Fig. 5b. In the near field, the two plots are nearly identical. However, it is now obvious that the average *TL* levels begin to increase beyond roughly 1/2 CZ (about 25 km). Taking the difference between these two data sets produces Fig. 6. As was suggested in the previous section, the transmission loss values actually appear lower (higher ensonification levels) within 1/2 CZ. Beyond this, the *TL* levels begin to increase more rapidly when azimuthal coupling is included.

The combination of these trends can be justified by the following argument. Without azimuthal coupling, all forward scattered energy is constrained to the 2-dimensional range/depth plane along each radial. When azimuthal coupling is included, forward scatter can spread energy into neighboring radials. Since this is true for all radials, the overall effect of forward scatter is an exchange of energy between radials at shorter ranges. This appears as an increase in average ensonification levels (lower *TL* values) within 1/2 CZ. Consequently, an increase in the energy interacting with the bottom at shorter ranges also results in a decrease in energy propagating to longer ranges. This appears as an overall decrease of ensonification levels (higher *TL* values) beyond 1/2 CZ. Note that this is not simply a loss of coherence due to forward scatter but is a true decrease in total energy due to an increase in bottom interactions near 1/2 CZ. This explanation is still highly speculative and warrants further study.

2. Effects on horizontal beam patterns

The effect of azimuthal coupling on horizontal beam patterns has been discussed previously by Tappert and Nghiem-Phu (1984). At issue is the standard approach used with horizontal receiving arrays of extending the receiver beam pattern out to long ranges for bearing localization. In the presence of strong azimuthal coupling, horizontal multipaths and "beam-splitting" may reduce the resolution of such arrays and contaminate the beam pattern at long ranges.

A depiction of this effect is shown in Fig. 7. Assume the beam pattern in the near field of the array is defined by $W(\theta)$. In the absence of azimuthal coupling, energy propagating along any radial θ will remain on that radial and it is justified to apply the near field beam pattern to all ranges. However, if energy is being transferred between radials, this is equivalent to a re-mapping of the beam pattern into $W'(\phi(r))$ which, in general, isn't known. This is analogous to the propagation from a vertical array in the sense that we cannot simply compute the field due to a point source and then attempt to impose the beam pattern on the solution.

An example of this is shown in Fig. 8. In each case, the horizontal starting field was a highly focused, Gaussian beam of width ~ 2°. In Fig. 8a, a 2DxN calculation is performed and, as expected, the beam remains highly focused with good angular resolution. When azimuthal coupling is included, however, the results displayed in Fig. 8b are significantly different. Even in the near field where we have usually found little distinction, there appears to be a significant amount of diffusion occurring into neighboring radials. With the amount of energy interacting with the bottom being spread among different azimuths at shorter ranges, we again find an overall decrease in energy levels at longer ranges. For a horizontal receiving array, the reciprocal

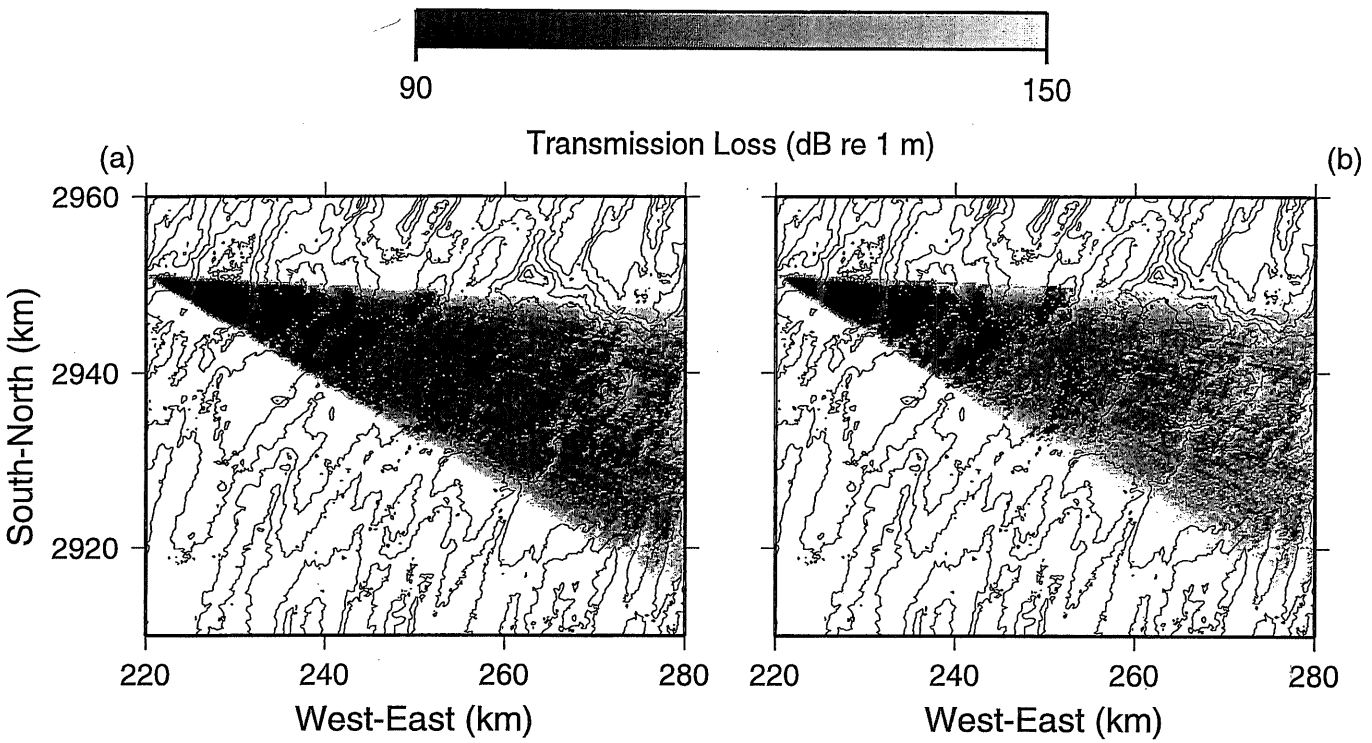

Figure 5: Transmission loss at bottom of deep ocean environment for 30 deg beam (a) without azimuthal coupling and (b) with azimuthal coupling.

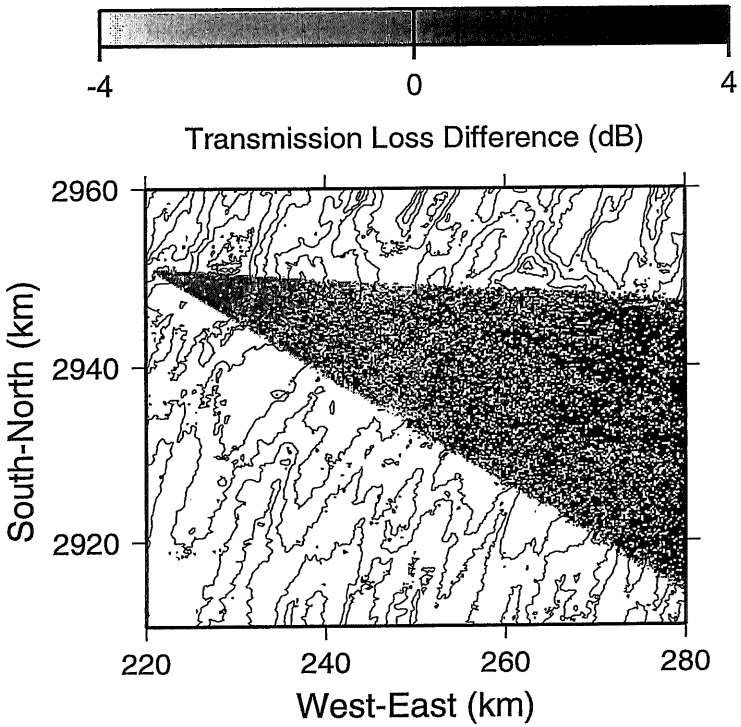

Figure 6: Difference in transmission loss values of Fig. 5(a) and 5(b). Positive values indicate higher TL with azimuthal coupling.

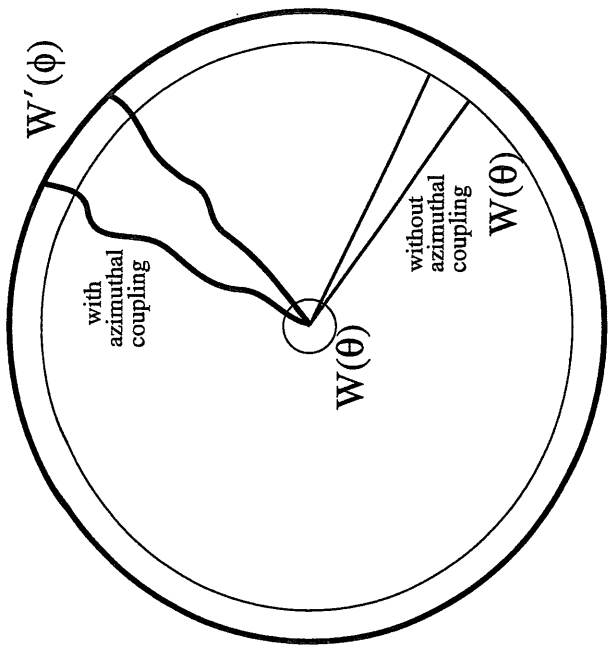

Figure 7: Schematic of azimuthal coupling influence on horizontal beam patterns.

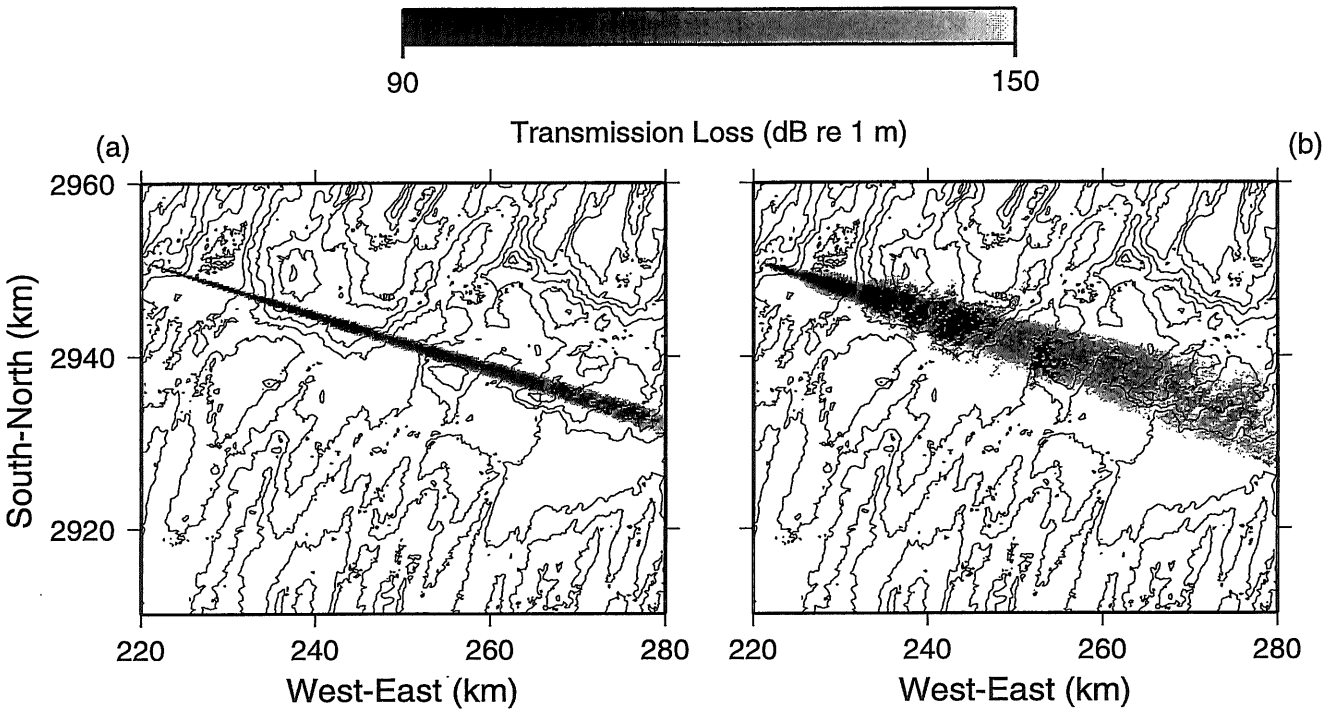

Figure 8: Transmission loss at bottom of deep ocean environment for 2 deg, high resolution beam (a) without azimuthal coupling and (b) with azimuthal coupling.

interpretation is that energy arriving along a narrow beam may have contributions from significantly distinct radials at long ranges.

IV. Summary

A reasonably simple method for incorporating azimuthal coupling into current split-step Fourier PE algorithms has been presented. In essence, it requires a 2-dimensional FFT of the PE field function between depth and vertical wavenumber and between azimuthal radial and an azimuthal wavenumber which has been defined. An azimuthal wavenumber operator is then employed within the SSF algorithm which serves to couple the radials. The result is a fully 3-dimensional PE propagation code. A "small angle" approximation of this operator was used and is consistent with the relatively small effects observed due to azimuthal coupling.

Two examples were then presented. The first was a simple, 3-dimensional wedge. The results exhibited the expected downslope refractive character for this environment. Direct confirmation with analytical solutions, however, has not yet been attempted. The second example was a realistic deep ocean environment using measured bathymetry as input. Part of the motivation here was to examine the influence of azimuthal coupling on the radial resolution of reverberation. It appears that in the presence of a rough bottom interface, the cross-range resolution is not accurate to more than several hundred meters at ± 5 dB or so for ranges of roughly 1/2 CZ and beyond. It also appeared that in the vicinity of 1/2 CZ, azimuthal coupling creates an overall increase in ensonification levels (decrease in *TL*). This result was treated cautiously, however, due to poor cross-range resolution at 1/2 CZ since only 512 radials were used to cover the entire 360°.

To examine this effect with decent cross-range resolution out to longer ranges, the total azimuthal coverage was reduced to 30° (with tapering to reduce the effect of side-lobes). Again, it appeared that the introduction of azimuthal coupling increases bottom ensonification levels near 1/2 CZ. Furthermore, it also seemed to decrease the overall ensonification levels at longer ranges. A simple argument was made to justify the physical cause of this. Further research is warranted to confirm this effect. It may then be possible to incorporate an effective bottom attenuation into 2DxN calculations to improve their accuracy.

Finally, the influence of azimuthal coupling on high-resolution horizontal beam patterns was also investigated. The accuracy of such high-resolution beams in the presence of rough boundaries seems to degrade rapidly. However, across several beams, the central radial may still serve as a good estimate for localization purposes.

Acknowledgments

The author would like to thank Brian Tucholke (WHOI) for providing the Hydrosweep bathymetry data used in our UMPE modeling. Thanks go also to Ching-Sang Chiu for the invitation to present this work. This research was supported by the Office of Naval Research.

References

Bottom/Subbottom Reverberation Science Plan (**1992**). ONR-ARSRP Symposium, La Jolla, CA, 7-9 April 1992.

Baer, R. N. (**1981**). "Propagation through a three-dimensional eddy including effects on an array," J. Acoust. Soc. Am. **69**, 70-75.

Berman, D. H., Wright, E. B. and Baer, R. N. (**1989**). "An optimal PE-type wave equation," J. Acoust. Soc. Am. **86**, 228-233.

Bowles, F.A. (**1994**). "A Geoacoustic Model for Fine-Grained, Unconsolidated Calcareous Sediments (ARSRP Natural Laboratory)," Naval Research Laboratory - Stennis Space Center, NRL Report.

Chin-Bing, S.A., King, D.B., Davis, J.A., and Evans, R.B., eds. (**1993**). "PE Workshop II: Proceedings of the 2nd Parabolic Equation Workshop, May 6-9, 1991," Naval Research Laboratory - Stennis Space Center, NRL Book Contribution.

Collins, M. D. (**1988**). "FEPE User's Guide," NORDA TN-365, Naval Ocean Research and Development Activity, Stennis Space Center, MS.

Deane, G. B. and Buckingham, M. J. (**1993**). "An analysis of the three-dimensional sound field in a penetrable wedge with a stratified fluid or elastic basement," J. Acoust. Soc. Am. **93**, 1319-1328.

Hardin, R.H. and Tappert, F.D. (**1973**). "Applications of the split-step Fourier method to the numerical solution of nonlinear and variable coefficient wave equations," SIAM Rev. **15**, 423.

Holmes, E. S. and Gainey, L. A. (**1991**). "Software product specification for the PE model, v.3.2," OAML-SPS-22 Naval Oceanography Office, Bay St. Louis, MS.

Lee, D. and Botseas, G. (**1982**). "IFD: An implicit finite-difference computer model for solving the parabolic equation," Rep. TR-6659, Naval Underwater Systems Center, New London, CT.

Smith, K.B. and Tappert, F.D. (**1993**). *UMPE: The University of Miami Parabolic Equation Model, Version 1.1*, MPL Technical Memorandum 432.

Tappert, F. D. (**1974**). "Parabolic equation method in underwater acoustics," J. Acoust. Soc. Am. Suppl. 1 **55**, S34.

Tappert, F.D. (**1977**). "The parabolic approximation method," in *Wave Propagation and Underwater Acoustics*, Lecture Notes in Physics, Vol. 70, edited by J.B. Keller and J.S. Papadakis (Springer-Verlag, New York), Chap. V, pp. 224-287.

Tappert, F. D. and Nghiem-Phu, L. (**1984**). "Receiver directivity modeling in three dimensions," J. Acoust. Soc. Am. Suppl. 1 **75**, S63.

Thomson, D.J. and Chapman, N.R. (**1983**). "A wide-angle split-step algorithm for the parabolic equation," J. Acoust. Soc. Am. **74**, 1848-1854.

Tucholke, B.E., Kleinrock, M.C., and Stewart, W.K. (**1993**). "Geological and Geophysical Characteristics of the Acoustic Reverberation Corridor and their Relevance to the Conduct of the G&G Fine-Scale Surveys," ONR-ARSRP Symposium, La Jolla, CA, 23-25 March 1993.